УДК 539.3

A. ZOLOCHEVSKY, Dr. Sc., ***N.N. TKACHUK,*** NTU "KPI",
J.-P. VIRICELLE, Dr., ***C. PIJOLAT,*** Dr., Ecole Nationale Supérieure des Mines de St-Etienne, France

CHEMICALLY INDUCED STRESSES IN THE CATHODE OF SINGLE CHAMBER SOLID OXIDE FUEL CELL

Установлено зв'язок між явищами дифузії іонів кисню, хімічним розширенням в електрохімічній кераміці та розвитком хімічно наведених напружень в часі в катоді твердооксидних паливних елементів з одним стеком мініатюрної конфігурації на базі тонких плівок у формі печатних плат. Розроблену модель використано для розрахунків залежних від часу розподілень напружень в катоді як функцій фізичних параметрів матеріалу, геометричних параметрів катоду та концентрації іонів кисню в сталих умовах роботи твердооксидних паливних елементів з одним стеком.

A relation between diffusion of the oxygen ions, chemical expansion in electrochemical ceramics, and chemically induced stress evolution in the cathode over time for the Single Chamber Solid Oxide Fuel Cell based on the miniaturisation concept using thick films produced by screen-printing method has been established. The proposed model has been used to calculate the time dependent stress distribution in the cathode as a function of the material parameters, geometrical parameters of the cathode, and concentration of the oxygen ions under steady state operating conditions of the Single Chamber Solid Oxide Fuel Cell.

Introduction. The concept of a Single Chamber Solid Oxide Fuel Cell (SC-SOFC) has been recently proposed by several groups of researchers in the world [1]. A SC-SOFC is an all solid state electrochemical device that operates at elevated temperatures in uniform mixtures of fuel and oxidant and can directly convert the chemical energy of the gas mixture into heat and electric energy by the use of reaction selective electrodes. In regards of conventional SOFC, the single chamber SOFC presents the high interest due to no need of seals in the SOFC system according to use of only one cell for both anode and cathode. The working principle of the SC-SOFC is based on a difference of catalytic activity of the electrodes resulting in preferential reactions with fuel or with air; the anode has a higher activity for fuel oxidation, whereas the cathode is more efficient for oxygen reduction.

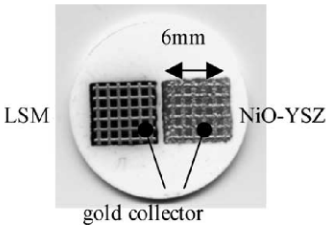

Fig.1. A Single Chamber Solid Oxide Fuel Cell [2]

The SC-SOFC configuration with conventional materials (anode made of NiO and yttria-stabilized zirconia YSZ, cathode made of Sr-doped lanthanum manganite LSM and solid electrolyte made from YSZ) is shown in Fig. 1 [2]. This SC-SOFC device is based on the thick films produced by screen-printing. The SC-SOFC under consideration refers to the so called SC-SOFCs with side by side placement of electrodes. A concept of

the SC-SOFC recently proposed in the Ecole Nationale Suprerieure des Mines (France) is based on the new materials: Gd or Sm doped ceria for the electrolyte, Ni or Cu composite materials (La_2NiO_4 or Nd_2CuO_4) for anode and $Ba_{0.5}Sr_{0.5}Co_{0.8}Fe_{0.2}O_3$ (BSCF) for the cathode. All materials are deposited by screen-printing using special inks prepared in the Ecole Nationale Suprerieure des Mines (France). The composition of the inks is adjusted in order to control the right properties of the inks. Mixtures of powders and organic precursors of these powders have been used to obtain suitable viscosities.

1. Mathematical model of the diffusion of oxygen ions. In the following, the constitutive and numerical modeling only of the cathode in the SC-SOFC under discussion will be considered. A mixture of O_2 and CH_4 is introduced from the outer surface of the cathode. The perovskite $Ba_{0.5}Sr_{0.5}Co_{0.8}Fe_{0.2}O_3$, material of the cathode, exhibits high oxygen ionic and electronic conductivity. The oxygen transport through cathode in the form of oxygen ions instead of oxygen molecules occurs, and oxygen ions diffuse from the outer surface of the cathode into the medium. The concentration, θ, of oxygen ions in the cathode follows Fick's second law and can be determined as [3]:

$$\theta = \theta_0 \left[\operatorname{erfc}\left(\frac{\alpha}{2\sqrt{Dt}} \right) \right], \qquad (1)$$

where α is the coordinate in the normal direction of the cathode, $\alpha \in [0, h]$; h is the thickness of the cathode; t is the time; θ_0 is the concentration of oxygen ions required to maintain equilibrium with the vapor pressure in the surrounding gas mixture remote from the outer surface of the cathode; D is the chemical diffusion coefficient of oxygen ions; $\operatorname{erfc} z$ is the complementary error function. As known, the error function

$$\operatorname{erf} z = \frac{2}{\sqrt{\pi}} \int_0^z \exp(-\eta^2)\, d\eta \qquad (2)$$

has the following properties

$$\operatorname{erf}(-z) = -\operatorname{erf} z\,;\ \operatorname{erf}(0) = 0\,,\ \operatorname{erf}(\infty) = 1\,.$$

Complementary error function is introduced as

$$\operatorname{erfc} z = 1 - \operatorname{erf} z = \frac{2}{\sqrt{\pi}} \int_z^\infty \exp(-\eta^2)\, d\eta\,;\ \operatorname{erfc}(0) = 1\,,\ \operatorname{erfc}(\infty) = 0\,. \qquad (3)$$

2. Modeling of chemically induced stresses. For the acceptor doped perovskite materials, for example, the cathode material $Ba_{0.5}Sr_{0.5}Co_{0.8}Fe_{0.2}O_3$, it is

well known that the unit cell volume changes with changes of stoichiometry [4]. Therefore the volume chemical expansion will lead to a build-up of chemically induced stresses in the cathode.

In the following, the cathode in SC-SOFC under discussion will be considered as a thin rectangular simply supported plate that occupies the domain

$$0 \le x \le a, 0 \le y \le b, -\frac{h}{2} \le z \le \frac{h}{2}$$

with the reference to the Cartesian coordinates (x, y, z). Here a and b are the sizes of the cathode in the plane.

The components of the total strains at the each point of the plate and at the each instant of the time can be calculated as a sum of the elastic parts, defined by the generalized Hooke's law, and chemically induced parts, i. e.

$$\begin{cases} \varepsilon_x = \dfrac{\sigma_x - \nu\sigma_y}{E} + \alpha_T\theta = -\dfrac{\partial^2 w}{\partial x^2} z + \varepsilon_x^m; \\ \varepsilon_y = \dfrac{\sigma_y - \nu\sigma_x}{E} + \alpha_T\theta = -\dfrac{\partial^2 w}{\partial y^2} z + \varepsilon_y^m; \\ \gamma_{xy} = \dfrac{2(1+\nu)}{E}\tau_{xy} = -\dfrac{\partial^2 w}{\partial x \partial y} z + \gamma_{xy}^m, \end{cases} \quad (4)$$

where σ_x, σ_y and τ_{xy} are stress components, E, ν and α_T are Young's modulus, Poisson's ratio and a new material constant related to the chemical expansion, respectively, w is the normal displacement of the middle plane of the plate, ε_x^m, ε_y^m and γ_{xy}^m are plane deformations of the points at the middle plane. Right parts in equation (4) correspond to the Kirchhoff hypothesis which we accept for the plate bending [5].

Since θ is a function of the coordinate z and horizontal displacements are not restricted at the boundary, middle plane is a homogeneously stretched one so that

$$\varepsilon_x^m = \varepsilon_y^m = \alpha_T \frac{1}{h} \int_{-h/2}^{h/2} \theta(z) dz, \ \gamma_{xy}^m = 0. \quad (5)$$

In order to exclude these strains from the further consideration an auxiliary balanced concentration function is introduced in the following form:

$$\bar{\theta} = \theta - \frac{1}{h} \int_{-h/2}^{h/2} \theta(z) dz. \quad (6)$$

This enables to express all the stress components in terms of the second derivatives of normal displacement w and oxygen ions concentration:

$$\begin{cases} \sigma_x = -\dfrac{E z}{1-\nu^2}\left(\dfrac{\partial^2 w}{\partial x^2} + \nu\dfrac{\partial^2 w}{\partial y^2}\right) - \dfrac{E}{1-\nu}\alpha_T\bar{\theta}; \\ \sigma_y = -\dfrac{E z}{1-\nu^2}\left(\nu\dfrac{\partial^2 w}{\partial x^2} + \dfrac{\partial^2 w}{\partial y^2}\right) - \dfrac{E}{1-\nu}\alpha_T\bar{\theta}; \\ \tau_{xy} = -\dfrac{E z}{1+\nu}\dfrac{\partial^2 w}{\partial x \partial y}. \end{cases} \quad (7)$$

According to these relations bending and twisting moments in the middle plane of the plate can be found as:

$$M_x = -D\left(\frac{\partial^2 w}{\partial x^2} + \nu\frac{\partial^2 w}{\partial y^2}\right) - M_\theta; \ M_y = -D\left(\nu\frac{\partial^2 w}{\partial x^2} + \frac{\partial^2 w}{\partial y^2}\right) - M_\theta;$$

$$M_{xy} = -D(1-\nu)\frac{\partial^2 w}{\partial x \partial y},$$

where D is the cylindrical stiffness of the plate, $D = \dfrac{E h^3}{12(1-\nu^2)}$,

$M_\theta = \dfrac{E}{1-\nu}\alpha_T \int_{-h/2}^{h/2} \bar{\theta}(z)\, z\, dz$.

These moments have to satisfy the equilibrium equation [5]

$$\frac{\partial^2 M_x}{\partial x^2} + 2\frac{\partial^2 M_{xy}}{\partial x \partial y} + \frac{\partial^2 M_y}{\partial y^2} = 0$$

and boundary conditions [5]

$$M_x = 0, x = 0, a; \quad M_y = 0, y = 0, b,$$

which enables to state a boundary value problem in regard to the normal displacement w:

$$\begin{cases} D\Delta w + M_\theta = 0 \\ w\big|_\Gamma = 0 \end{cases}. \quad (8)$$

Exact solution of the boundary value problem given by equation (8) is delivered by an infinite series

$$w(x,y) = \frac{4M_\theta}{\pi D} \sum_{n=1,3,..} \frac{1}{n\alpha_n^2}\left[1 - \frac{\operatorname{ch}\alpha_n(y - \frac{b}{2})}{\operatorname{ch}\frac{\alpha_n b}{2}}\right]\sin\frac{\pi n x}{a}, \quad (9)$$

where $\alpha_n = \frac{\pi n}{a}$. This series converges together with its second derivatives, which enables to substitute their values in equation (7) and to obtain sought stresses at all points of the cell at all instants of the time, i.e.

$$\sigma_x = \frac{12z}{h^3} M_\theta \left[1-(1-\nu) \sum_{n=1,3,..} \frac{4}{\pi n} \frac{\operatorname{ch} \alpha_n (y-\frac{b}{2})}{\operatorname{ch} \frac{\alpha_n b}{2}} \sin \frac{\pi n x}{a} \right] - \frac{E}{1-\nu} \alpha_T \bar{\theta};$$

$$\sigma_y = \frac{12z}{h^3} M_\theta \left[\nu+(1-\nu) \sum_{n=1,3,..} \frac{4}{\pi n} \frac{\operatorname{ch} \alpha_n (y-\frac{b}{2})}{\operatorname{ch} \frac{\alpha_n b}{2}} \sin \frac{\pi n x}{a} \right] - \frac{E}{1-\nu} \alpha_T \bar{\theta}; \qquad (10)$$

$$\tau_{xy} = \frac{12z}{h^3} (1-\nu) M_\theta \sum_{n=1,3,..} \frac{4}{\pi n} \frac{\operatorname{sh} \alpha_n (y-\frac{b}{2})}{\operatorname{ch} \frac{\alpha_n b}{2}} \cos \frac{\pi n x}{a}.$$

Note that the concentration of oxygen ions θ in equations (8), (10) is given by equation (1).

3. Numerical results. The model described above was employed to determine chemically induced stresses in a cathode of the SC-SOFC at 973K. Values of parameters have been taken as follows: concentration of oxygen ions at the equilibrium is $\theta_0 = 0.056$, chemical expansion factor is $\alpha_T = 0.00489$, chemical diffusion coefficient of oxygen ions is $D = 0.246 \cdot 10^{-8} \frac{\text{m}^2}{\text{s}}$ [6], Young's modulus and Poisson's ratio are $E = 100\,\text{GPa}$ and $\nu = 0.3$ [7], the sizes of the plate are a=0.005 m and b=0.01 m, thickness of the plate h=2 $\cdot 10^{-5}$ m.

Fig. 2 shows the distribution of oxygen ions concentration across a thickness of the plate as a function of time according to equation (1). It is seen that the concentration at any point of a plate except point with z=h/2 increases with increasing time. Furthermore, the most intensive growth of oxygen ions concentration with increasing time occurs up to 1s, and the instant at 1s can be accepted as the equilibrium time.

The gradient of the concentration of oxygen ions in perovskite material leads to the appearance of the diffusion-induced stresses in a cathode. High levels of these stresses can be a source of the cathode cracking in the SC-SOFC. Therefore, in the following we will estimate the development of diffusion- induced stresses with time using Eq. (10) and material constants given above.

As known, mechanical failure of perovskite material includes fracture and permanent straining caused by domain switching of this perovskite. Figs. 3-6 show the distribution of the chemically induced stresses at the centre of a cathode.

Fig. 3a shows the redistribution of the stress σ_x across a thickness of the cathode with time. It is seen that the stress σ_x is compressive in the region near the boundary surfaces $z = \pm h/2$ at the centre of a cathode and tensile in the middle region of a cathode, and that the absolute value of the maximum level corresponds to a compressive stress. Starting at the instant of time t =1s we have approximately zero stresses σ_x at the centre of a cathode.

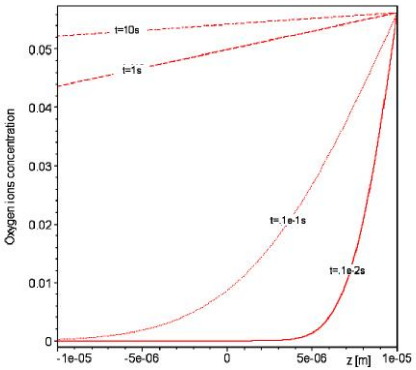

Fig. 2. The distribution of oxygen ions concentration across a thickness of the cathode with time

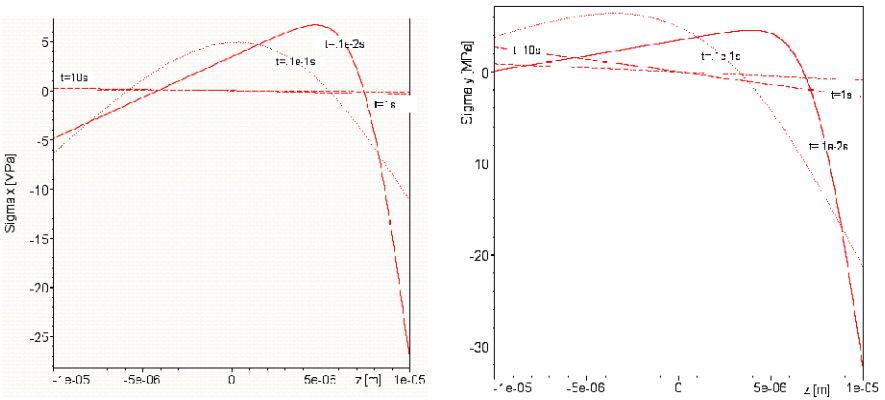

a b

Fig. 3. The distribution of the stress components σ_x (a), σ_y (b) across a thickness with time at a centre of the cathode

It is clear from Fig. 3b that the stresses σ_y are positive (tensile) for all moments of time at each point of a cathode at its centre except for the outer of its surface $z = h/2$. Starting at the instant of time t =1s we have small values of stresses σ_y at the centre of a cathode due to the stress relaxation with time.

Thus, the results above show, as oxygen ions diffuse into perovskite structure, tensile stresses arise in the interior of the sample. The probability of a crack due to

tensile failure in the middle region of a cathode is increasing during the initial period of the diffusion. To demonstrate that the distribution of the first principal stress across a thickness of the cathode as a function of time is considered (Fig. 4). It is seen, for example, that at the centre of the cathode the maximum value of the first principal stress $\sigma_1 = 6.7\text{MPa}$ is reached at $t = 0.001\text{s}$, and then the stress relaxation process develops. In this regard, there is here the risk of a crack formation in the cathode during the initial period of the diffusion when the first principal stress reaches the strength limit of the perovskite material under tension.

The penetration of oxygen ions causes also a change in the direction of the first principal stress distribution (Fig. 4). The first principal stress in the region with the positive values of the coordinate *z* except for the outer of boundary surface $z = h/2$ coincides with the orientation of the stress σ_x, and microcracks form and propagate perpendicular to the direction *x*. In the region of a cathode with the negative values of the coordinate *z* the first principal stress is related to the direction of the stress σ_y, and microcracks can form and propagate perpendicular to the direction *y*. The position of the point with coordinate *f* where the maximum value of the first principal stress at the centre of a cathode occurs changes with time under point moving from the region near the outer surface to the inner surface (Fig. 5).

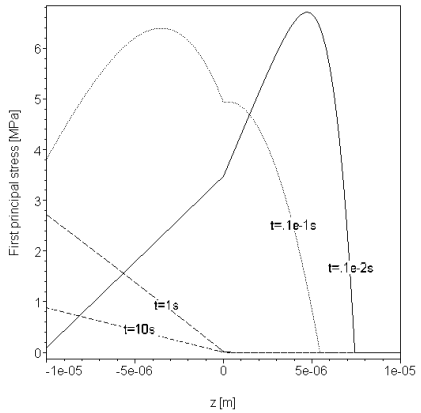

Fig. 4. The distribution of the first principal stress σ_1 across a thickness with time at a centre of the cathode

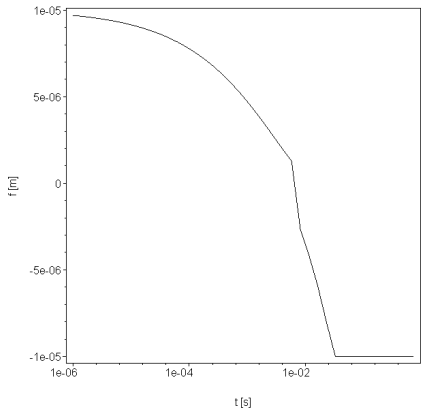

Fig. 5. Drift of the location of the point with coordinate *f* with the maximum value of the first principal stress across a thickness with time at a centre of the cathode

On the other hand, the highest compressive stresses at a centre of the cathode arise at the boundary surface $z = h/2$. The condition of permanent straining has a form

$$\sigma_i > \sigma_c \qquad (11)$$

where σ_i is the von Mises equivalent stress, and σ_c is the limit of the linear elasticity under compression,

$$\sigma_i = \sqrt{\sigma_x^2 - \sigma_x\sigma_y + \sigma_y^2}\,. \qquad (12)$$

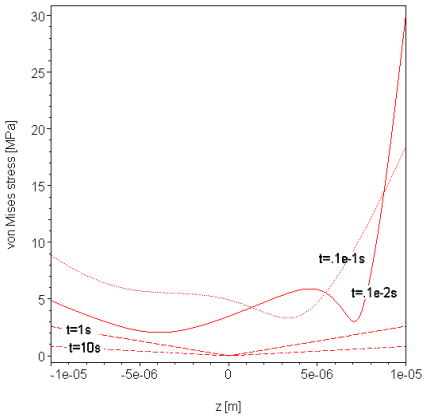

Fig. 6. The distribution of the von Mises stress σ_i across a thickness with time at a centre of the cathode

It is seen from Fig. 6 that the von Mises stress has the maximum value at the outer surface and at $t = 0.001\text{s}$. A fracture based on a shear crack will appear in a cathode of the SC-SOFC when the maximum von Mises stress exceeds the strength limit of the material under compression.

4. Conclusion. A predictive tool which is able to reproduce the chemically induced stresses in a cathode of the SC-SOFC has been proposed. Within the proposed approach it is possible to investigate the effect of oxygen stoichiometry related to the partial oxygen pressure as well as of the sizes of the cathode and its thickness on the level of the chemically induced stresses.

A picture of the stress evolution over time in the entire SC-SOFC system (cathode- solid electrolyte- anode) is more complicated. The chemical expansion of the cathode material and densification of the electrolyte will lead to a build-up of chemically induced stresses in the SC-SOFC that can be a source of the failure of the whole system as well as of its degradation over time.

For example, Fig. 7 shows the difference between the calculated and experimentally measured open circuit voltage (OCV) for anode-supported SC-SOFC of the conventional design with electrodes on each side of a dense electrolyte operating on the gas mixtures characterized by the ratio of CH_4 and O_2 denoted as x [1]. The calculated OCV values have been obtained under assumption of perfect electrodes and purely ionic conducting electrolyte. In fact, the chemical expansion of the cathode material and densification of the electrolyte occur that can be a source of the SC-SOFC degradation over time. Therefore, it is necessary to introduce the more realistic model for the OCV calculations taking into account the diffusion of oxygen ions, appearance of the chemically induced stresses and degradation of the SC-SOFC system over time.

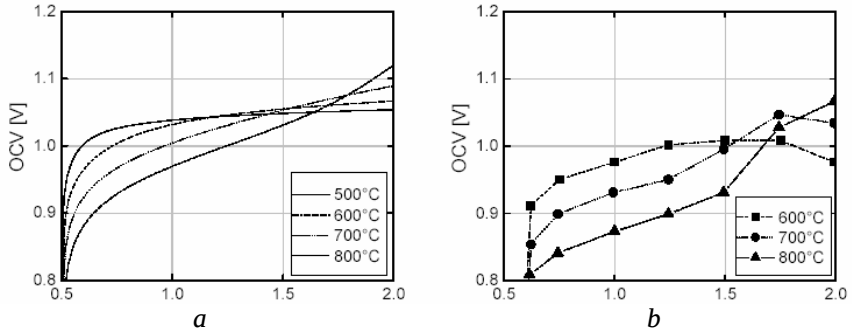

Fig. 7. The calculated and experimentally measured open circuit voltage (OCV) for SC-SOFCs operating on CH_4 -air mixtures with different x-ratio of CH_4 and O_2 [1]:
a – calculated OCV for SC-SOFCs, assuming perfect electrodes and purely ionic conducting electrolyte,
b – experimentally measured OCVs of anode-supported SC-SOFCs with YSZ-electrolyte

Another example shown in Fig. 8 demonstrates the difference between the OCV data measured during heating and cooling for electrolyte-supported SC-SOFC of the conventional design with electrodes on each side of a dense electrolyte. The SC-SOFC is produced by screen-printing method. It is seen from Fig. 8 that the OCV during cooling was generally lower than during the heating stage. Obviously, the permanent straining and irreversible change of the anode material occur during the temperature cycle and serve as a source of the SC-SOFC degradation over time.

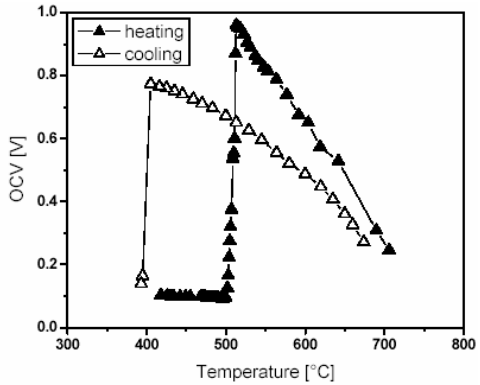

Fig. 8. The experimentally measured open circuit voltage (OCV) of a SC-SOFC with 0.19 mm thick electrolyte as a function of temperature with 380 ml/min methane and 260 ml/min airflow during heating with 2 K/min and cooling with 5 K/min [1]

The analysis of the stress and damage evolution in a SC-SOFC with time can be produced according to an integrated approach proposed earlier in [8] using ANSYS software. In this way, it is possible to study the SC-SOFC degradation over time influenced by:

- SC-SOFC design type,
- the gap between the two electrodes in a SC-SOFC planar design with side by side placement of electrodes,
- the gas flow rate, the gas flow configuration, the gas composition and the operating temperature,
- the current-collectors effect,
- the thickness of the anode layer and the electrolyte layer,
- shapes, geometries and electrochemical properties of the electrodes,
- permanent straining and irreversible change of the anode material,
- densification of the electrolyte,
- oxygen stoichiometry of the cathode material,
- thermal gradient across a thickness of the SC-SOFC,
- creep effect.

The research described in this paper was sponsored by the Ministry of Education and Science of the Ukraine and EGIDE within the framework of the scientific cooperation between Ukraine and France based on the programme “Dnipro”. The first author would like to thank Madam Sakharenko T.O. for useful advices and cooperation.

References: 1. *Bürgler B.E.* Single chamber solid oxide fuel cells. Ph.D Thesis, Swiss Federal Institute of Technology, Zurich. – 2006. **2**. *Rotureau D., Viricelle J.-P., Pijolat C., Caillol N., Pijolat M.* Development of a planar SOFC device using screen-printing technology. Journal of the European Ceramic Society. – 2005. – 25. – PP.2633-2636. **3**. *Crank J.* The mathematics of diffusion. Second edition. – Oxford: Oxford University Press, 1999. **4**. *McIntosh S., Vente J.F, Haije W.G., Blank D.H.A., Bouwmeester H.J.M.* Oxygen stoichiometry and chemical expansion of $Ba_{0.5}Sr_{0.5}Co_{0.8}Fe_{0.2}O_{3-\delta}$ measured by in situ neutron diffraction. Chem. Mater. – 2006. – 18. – PP.2187-2193. **5**. *Timoshenko S P, Goodier J N.* Theory of elasticity. Third edition. – New York: McGraw-Hill, 1970. **6**. *Wang H., Yang W., Tablet C., Caro J.* Oxygen diffusion in oxide crystals - Tracing new routes to identify the rate limiting step of oxygen permeation through perovskite membranes. – Diffusion Fundamentals. – 2005. – 2. – PP.46.1-46.15. **7**. *Vente J.F., McIntosh S., Haije W.G., Bouwmeester H.J.M.* Properties and performance of $Ba_xSr_{1-x}Co_{0.8}Fe_{0.2}O_{3-\delta}$ materials for oxygen transport membranes. // J Solid State Electrochem. – 2006. – 10. – PP.581-588. **8**. *Zolochevsky A. A., Hyde T.H., Hu Zhaoji.* An integrated approach to the analysis of creep, chemical expansion, creep damage and lifetime reduction for solid oxide fuel cells //Вісник НТУ «ХПІ». Тематичний випуск «Машиноведение и САПР». – 2007. – № 3. – С. 151-159.

Поступила в редколлегию 19.05.07

СОДЕРЖАНИЕ

Е.Н. БАРЧАН Совершенствование конструкции выбивной машины в составе автоматизированной линии крупного вагонного литья на основе расчетно-экспериментальных исследований рабочего процесса ……..... 3
Е.Н. БАРЧАН, В.А. ШКОДА, В.В. ПРОСЯНОК, А.В. ГРАБОВСКИЙ Экспериментальное исследование динамических процессов в оптимизированной выбивной машине …… 26
Ю.Б. ГУСЕВ, В.А. ШКОДА, А.Ю. ТАНЧЕНКО Формирование конечно-элементной модели металлоконструкции углеперегружателя …..……..…… 33
Н.А. ДЕМИНА, О.П. НАЗАРОВА, А.Н. ТКАЧУК Контактное взаимодействие в сопряжении „пуансон – штампуемый материал – матрица”..... 39
І.В. КУЗЬО, А.Б. БІЛОУС Моделювання роботи маятникового вібратора при змішаному збуренні ……..…….. 48
В.И. КОХАНОВСКИЙ, О.В.КОХАНОВСКАЯ К вопросу оптимизации параметров оптической системы светодиодного шахтного светильника …… 52
А.Ю. ЛАРИН, А.В. МАРТЫНЕНКО Моделирование картины напряженности электрического поля в устройстве электродинамического воздействия при помощи пакета ANSYS/EMAG ……..... 67
А.Г. ПРИЙМАКОВ, А.В. УСТИНЕНКО, В.Н. СТАДНИЧЕНКО Износостойкость несущих поверхностей зубчатых передач ……. 74
Н.А. ТКАЧУК, Г.Д. ГРИЦЕНКО, А.В. МАРТЫНЕНКО, А.В. НЕЧЕПУРЕНКО, Т.В. ПОЛИЩУК К вопросу расчетно-экспериментального исследования элементов сложных механических систем ……...…...……...… 81
Н.А. ТКАЧУК, Г.Д. ГРИЦЕНКО, А.В. НЕЧЕПУРЕНКО, В.И. ГОЛОВЧЕНКО, В.А. ШКОДА Структура специализированных систем автоматизированного анализа и синтеза сложных механических конструкций ……. 93
Н.А. ТКАЧУК, В.К. ПИОНТКОВСКИЙ, В.Ю. ФЕДАК, Ю.В.ВЕРЕТЕЛЬНИК К вопросу о расчетно-экспериментальном исследовании напряженно-деформированного состояния биомеханических систем …….. 99
А.Д. ЧЕПУРНОЙ, А.В. ЛИТВИНЕНКО, И.В. АРТЕМОВ Автоматизированное проектирование карт раскроя, подготовки и выпуска управляющих программ для машин термической резки в производстве бронедеталей корпусов и башен БТР……... 121
A. ZOLOCHEVSKY, A. KÜHHORN Constitutive and numerical modeling of chemical and mechanical phenomena in solid oxide fuel cells and oxygen permeable membranes 128
A. ZOLOCHEVSKY, G. THIAGARAJAN An integrated approach to assessing seismic simulation based on analysis of preseismic, coseismic, postseismic and interseismic creep, and creep damage evolution……... 139
A. ZOLOCHEVSKY, N.N. TKACHUK, J.-P. VIRICELLE, C. PIJOLAT Chemically induced stresses in the cathode of single chamber solid oxide fuel cell…….. 148

НАУКОВЕ ВИДАННЯ

ВІСНИК
НАЦІОНАЛЬНОГО ТЕХНІЧНОГО УНІВЕРСИТЕТУ „ХПІ”

Тематичний випуск
“МАШИНОЗНАВСТВО та САПР”

Збірник наукових праць
№ 23

Науковий редактор
Ткачук М.А.

Технічний редактор
Ткачук Г.В.

Відповідальний за випуск
Обухова І.Б.

Обл. вид. № 128-07.

Підп. до друку 10.09.2007 р. Формат 60х90/16. Папір офісний.
Віддруковано на ризографі. Гарнітура Таймс. Ум. друк. арк.8,1.
Обл.-вид. арк.9,8. Тираж 300 прим. Зам. № 273.

Надруковано СПД ФО Ізрайлев Є.М.
Свідоцтво № 04058841Ф0050331 від 21.03.2001 р.
61024, Харків, вул. Гуданова, 4/10.